

GT2005-68835

INFLUENCE OF SWEEP ON THE 3D SHOCK STRUCTURE IN AN AXIAL TRANSONIC COMPRESSOR

Jörg Bergner, Stephan Kablitz, Dietmar K. Hennecke

Gas Turbines, Flight- and Space Propulsion
Technische Universität Darmstadt
Petersenstrasse 30
D-64287 Darmstadt, Germany
bergner@glr.tu-darmstadt.de

Harald Passrucker, Erich Steinhardt

MTU Aero Engines GmbH
Dachauer Strasse 665
D-80995 München, Germany
harald.passrucker@muc.mtu.de

ABSTRACT

To improve the understanding of how sweep affects the 3D shock structure and the shock-vortex interaction, two transonic compressor bladings are measured with a 3D Laser-2-Focus setup, and the flow is analyzed for comparable operating conditions. Rotor 1 features radially stacked profiles, while rotor 3 introduces forward sweep.

Performance comparisons of these rotors [1] indicated that forward sweep, as introduced in this design, has a beneficial effect on performance and stall margin.

The detailed experimental analysis of the 3D shock structure and the influence of tip leakage vortex interaction at design speed is the scope of this paper.

NOMENCLATURE

Blisk	bladed disk
L2F	Laser-2-Focus
Ma _{rel}	relative Mach number
NS	near stall
PE	peak-efficiency
RANS	Reynolds-averaged Navier-Stokes

INTRODUCTION

Initially, the intention for introducing sweep to the rotor blades of axial transonic compressors was to influence the inclination of the passage shock. However, recent investigations revealed that in the outermost tip region of the blading, the flow physics prevent translation or inclination of the shock [2].

One explanation of the effect on performance and stall behavior of sweep is the impact of sweep on the interaction of the tip leakage vortex and the passage shock. While the shock position remains unchanged, the tip leakage vortex can be influenced by sweep of the blade tip region.

As shown by Denton and Xu [2], if the tip of a blade is swept forward, the loading of the tips leading edge is reduced, thus resulting in a decreased tip leakage flow.

Based on the geometry of the original rotor 1, whose design dates back to the early 1990s [3], a new rotor – hereafter designated as rotor 3 – was designed in 2001 featuring pronounced forward sweep.

Experimental results presented by Passrucker et al. [1] underpinned the design intent. The predicted increase in efficiency was confirmed, but the operational range was significantly wider than expected.

Inspired by Wilke and Kau [4], Kablitz et al. [5] investigated the phenomenon of vortex breakdown due to vortex-shock interaction, which is believed to be one of the main triggers for stall inception.

As the compressor is throttled, the shock becomes stronger, moves upstream and it becomes difficult for the vortex to pass the shock unaltered. At a certain operating condition the driving pressure difference falls below a critical level, and vortex breakdown occurs with low momentum fluid blocking the passage in the whole tip region and eventually reaching the adjacent blade and spilling over into the next passage.

One approach to delay vortex breakdown is to increase the distance between the point where the vortex builds up at the suction side of the blade-tip and its intersection with the passage shock. The longer this distance between the upstream vortex and the shock, the more reenergisation of the vortex-core – increasing the total-pressure within – can take place.

As reported in [6] the evaluation of the pressure ratio between the minimum relative total pressure inside the vortex-core just upstream the shock and the average static pressure downstream of the rotor passage for both rotor configurations showed significantly higher pressure ratios for rotor 3 throughout the investigated operation range.

In this paper experimental data acquired by using a 3D-Laser-2-Focus system with both the conventionally stacked and the forward swept rotor is analyzed. In addition, the experimental data is compared to numerical results for both rotors.

Since the performance of high speed transonic compressor rotors can be very sensitive to changes in blockage [7], the shock/boundary-layer interaction of rotor 3 is discussed as well.

TEST FACILITY

The Department of Gas Turbines, Flight and Space Propulsion at Technische Universität Darmstadt has been operating the transonic compressor rig – which represents a typical front-stage of a commercial turbofan high-pressure compressor – since the early 1990s. Table 1 lists the design parameters of the test stand [3]. The main purpose of the test stand is to establish a database for CFD code validation as well as to serve as a test bed for new materials. Until today four different rotor geometries have been investigated.

Figure 1 gives an overview of the test stand. The ambient air is led through a settling chamber and a bell mouth - calibrated for mass flow rate determination - into the compressor stage. The rotor is driven by a 800 kW DC-drive, shaft speed is increased to the design speed of 20,000 rpm by a gearbox. Shaft speed and torque are measured by a torquemeter device.

Details of the standard instrumentation, postprocessing and measurement uncertainties are given in [5].

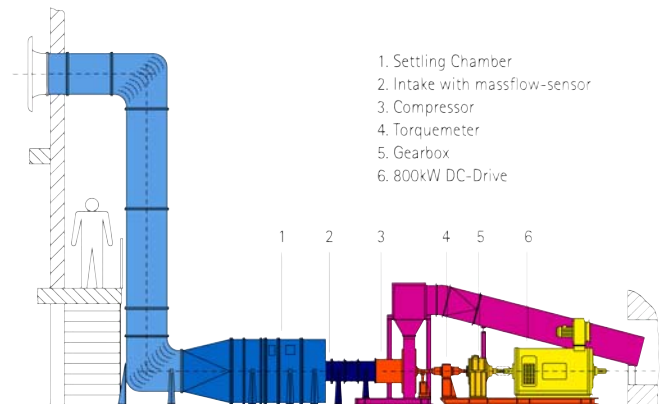


Figure 1 Sketch of the installation

pressure ratio	1.5
corrected mass flow rate	16 kg/s
corrected tip speed	398 m/s
rel. rotor inlet Mach number at tip	1.35
rel. rotor inlet Mach number at hub	0.70
shaft speed	20,000 rpm
tip diameter	0.38 m
inlet hub to tip ratio	0.51

Table 1 Compressor design parameters [3]

INVESTIGATED ROTOR GEOMETRIES

Compared to the baseline design rotor 1 shown in Fig. 2, rotor 3 features 14 instead of 16 blades and increased chord length towards the tip in order to maintain solidity (Fig. 3).

The measured tip gap of rotor 1 and rotor 3 is 0.9 mm and 0.7 mm (corresponding to 0.95% and 0.74% of mean blade span), respectively.

Both rotors are operated with the same stator, consisting of 29 blades. It was designed together with rotor 1 in 1993. Further information on the geometric properties are given in [1] and [3].



Figure 2 Rotor-1: Radially stacked blisk



Figure 3 Rotor-3: Forward swept blisk

3D LASER-2-FOCUS SETUP

To measure the flow field in the rotor, the 3D laser-2-focus (L2F) system of DLR in Cologne was applied. The system uses two independent single L2F systems, which are at a defined angle to each other, thus allowing to record the velocity component in the spanwise direction [8]. Being a statistical method, information on the turbulence intensity is also collected. The system is capable of detecting particles as small as $0.1 \mu\text{m}$. The laser beams have a diameter of $10 \mu\text{m}$ and their distance can be varied between $70 \mu\text{m}$ - $400 \mu\text{m}$ to account for different turbulence intensities of the flow.

No distinction is made between individual blade passages, so the measured values for velocity, flow angle, and degree of turbulence are mean values for the entire rotor at the specified position.

In order to increase data acquisition rates and thus to reduce operating time, seeding with dispersed paraffin oil was applied. The oil was injected into the flow in the settling chamber (see Fig. 1). The position far upstream of the rotor was chosen to minimize the influence of the probe on the flow.

A simple seeding injector, consisting of a pipe with a diameter of 12 mm, bent 90° in the direction of the flow at the end, was used. Readjustments of the injector in response to the probe-volume position provided optimum seeding for each reading. Since the size of the particles was smaller than $0.5 \mu\text{m}$, the velocity lag of these particles in the shock region can be neglected.

The measurement grids on which nodes' data was gathered are shown in Fig. 4 and Fig. 5 for rotor 1 and rotor 3, respectively. In contrast to the L2F measurements of rotor 1 back in 1995, where several operating points and different speeds were examined, for rotor 3 only measurements at „near stall“ (NS) and „peak-efficiency“ (PE) at design speed were taken. Thus a refined grid could be used. As can be seen from Tab. 2, for rotor 3 the number of measurement positions more than tripled.

The relative Mach number is calculated from the relative velocity and the local speed of sound at each point in the flow field by using an approximation described in [9].

The accuracy of measured velocities and angles - depending on turbulence intensity, beam separation and number of transits recorded - can be determined to be smaller than 1% for velocities and 0.1° - 0.3° for flow angles.

Despite the high precision of the system, if the turbulence intensity at a certain position is too high, the properties of the flow cannot be reliably determined. These positions are for example the red marks in Fig. 11. Due to the coarse grid of rotor 1 the blade shadow region appears to be much larger than for rotor 3 (Fig. 8).

Rotor	No. 1	No. 3
radial positions	5	10
axial positions	12	21
circumferential positions	16	16
total	960	3360

Table 2 Dimensions of L2F grid

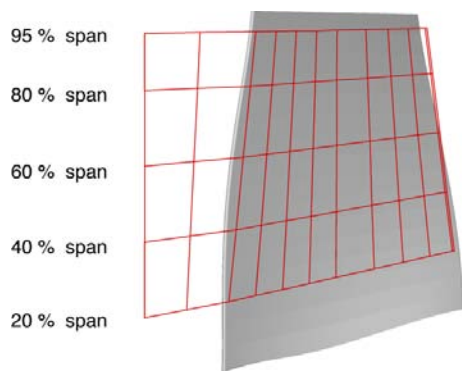


Figure 4 3D-L2F grid Rotor-1

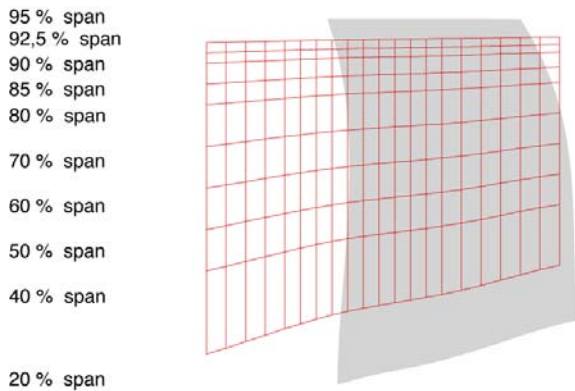


Figure 5 3D-L2F grid Rotor-3

COMPUTATIONAL PROCEDURE

Trace_S, an explicit cell-centered 2nd-order-accurate finite-volume scheme was used to solve the Reynolds-averaged Navier-Stokes equations. To speed up convergence to steady-state, local time-stepping, residual smoothing and successive mesh refinement are applied [10].

A high Reynolds' $k-\epsilon$ model with wall functions was used. ISA standard conditions with purely axial flow were assumed at the inflow. A rather pronounced incoming casing boundary layer, based on experimental data, was prescribed via a total pressure profile.

A block-structured O-H grid was used with a total of 630'000 nodes. Grid density is refined at hub and casing to increase the resolution of the boundary layers as well as the passage shock. Information between the rotor and stator domain is transferred by a mixing-plane interface. The numerical grid is shown in [1].

RESULTS AND DISCUSSION

Compressor map

Measured and calculated performance maps of the stage at design speed are presented in Fig. 6. Pressure ratio and efficiency are well calculated for both rotors. Rotor 3's pressure ratio is increased throughout the whole speedline and a better efficiency at design point could be achieved.

The experimentally obtained speedlines contain the last stable operating points of each rotor before stall. The substantially improved flow range of rotor 3 is significantly wider than predicted by the calculations. Some of this improvement, as well as some of the increase in efficiency, must be attributed to the about 0.2% span smaller tip gap of rotor 3 and the increased chord at tip that, in addition to the forward sweep, helps to unload the tip.

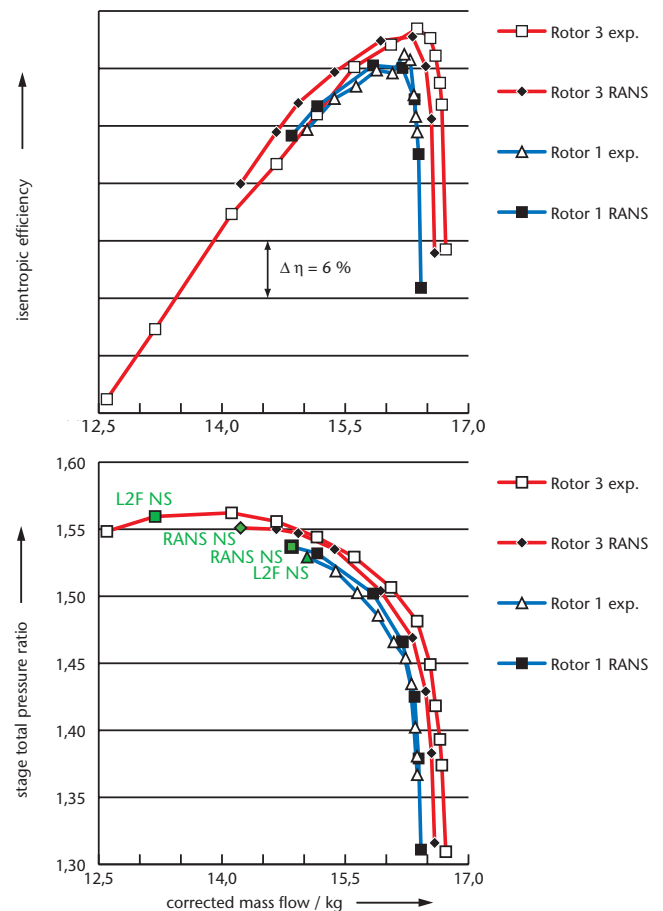


Figure 6 Stage performance at design speed

Computational results

To supplement the experimental data, computational results generated for operating conditions at „peak efficiency“ and „near stall“ are presented first.

The same color bar with a range from 0.1 - 1.6 is used for all Mach number contours throughout this paper.

Predicted relative mach number contours are shown in Fig. 7 and Fig. 10 at 95% channel height. At first glance, shock structures appears to be similar for both rotors. The passage shocks are oblique and attached to the leading edge at „peak efficiency“. At „near stall“ the shocks are almost normal to the blade and detached from the leading edge.

But pre-shock Mach numbers are somewhat higher for both rotors at „near stall“. More important, at „peak efficiency“ the passage shock of rotor 3 is more oblique.

At „near stall“ the shocks of both rotors are distorted at mid pitch, where the tip clearance vortex intersects the shock.

For both rotors a region of low Mach number fluid emerges near mid pitch downstream of the passage shock and migrates toward the pressure side at the blades' trailing edge.

Experimental results

Fig. 8 and Fig. 11 show the measured relative Mach number, Fig. 9 and Fig. 11 show the flow angle in radial direction beta at 95% channel height flattened to a plane of constant radius. Due to the high level of unsteadiness of the flow in the tip region and thus increased data acquisition time, this is the outermost plane in which measurements were taken.

No attempt was made to smooth the experimental data, since for example interpolation on a fine grid could reduce the information contained. Therefore the measurement grid has to be kept in mind when interpreting the contour plots.

Due to the coarse grid used for rotor 1, the shock front seems to be jagged but with respect to the numerical results (Fig. 7) shock location, pre-shock Mach number and the overall flow field are in good agreement for both operating conditions (Fig. 8).

The L2F data of rotor 3 instead is much finely resolved (Fig. 11). This is best seen when the blade shadow regions are compared to those of rotor 1. At this measurement plane of 95% span, the red marks indicate areas in which no meaningful readings could be taken due to a high turbulence level.

The high Mach number region at the pressure side near leading edge at „peak efficiency“ was only measured at 95% span. In the plane just below, at 92.5% span, this could not be observed and the shock front is oblique as predicted by the numerical simulation. The predicted higher pre-shock Mach number levels of both rotors at „near stall“, especially close to the suction side, are confirmed by the measurements.

The low Mach number region downstream of the shock for „near stall“ condition as predicted for both rotors could only be verified for rotor 1. Instead, the measurements of rotor 3 at „near stall“ show a strong distortion of the shock close to the suction side and an area of low Mach number at trailing edges suction side, but no low Mach number region as predicted by the numerical simulation.

From Fig. 9 and Fig. 11 it can be clearly seen, how the strength of rotor 3's tip clearance vortex could be reduced, especially at „peak-efficiency“. Interestingly the vortex, despite being quite pronounced at „near stall“, does not lead to a significant area of low momentum fluid downstream of the shock.

To assess this further, Fig. 13 shows Mach number contours together with velocity vectors in the relative frame of reference for „near stall“ condition at 92.5% and 95% span.

At 92.5% span a very small low Mach number region close to the pressure side is slightly visible. But it appears that the flow just downstream of the passage shock, still far way from the low Mach number region, is deflected towards the pressure surface and thus leading to an increased incidence angle at the blades' leading edge. At 95% span the strength of the tip clearance vortex upstream of the shock leads to a deflection of the flow towards the suction side. After passing the shock this flow turns abruptly towards the pressure side giving rise for the separation at trailing edge.

It is remarkable how the trajectory of the tip clearance vortex is deflected towards the pressure side after crossing the passage shock as can be seen in Fig. 13.

PEAK EFFICIENCY

NEAR STALL

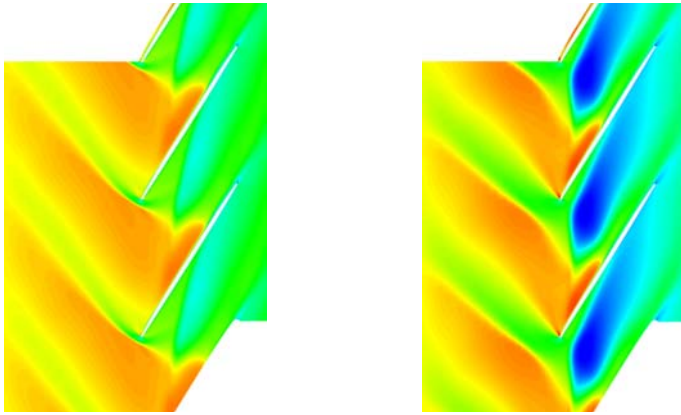


Figure 7 Relative Mach number contour of rotor 1 at 95% span (Numerical data)

PEAK EFFICIENCY

NEAR STALL

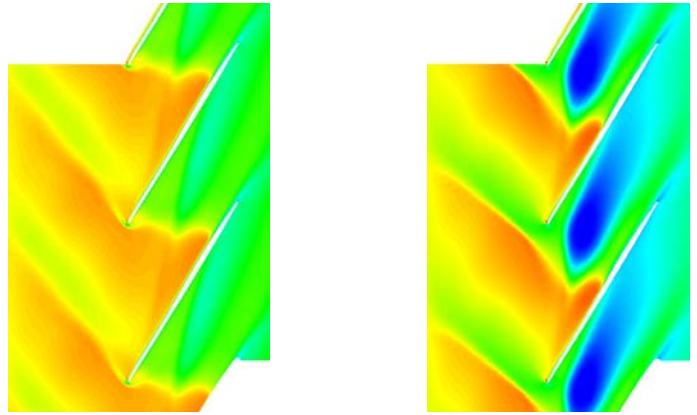


Figure 10 Relative Mach number contour of rotor 3 at 95% span (Numerical data)

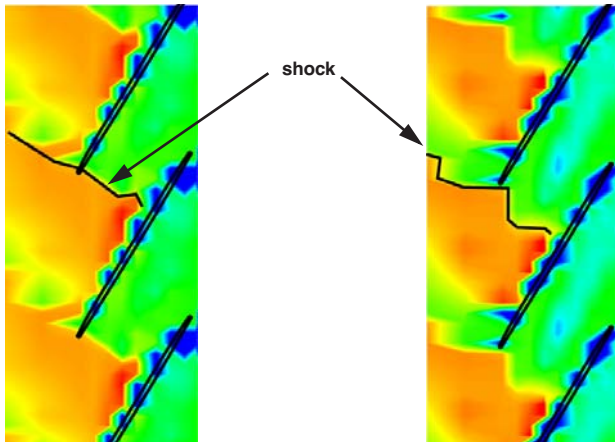


Figure 8 Relative Mach number contour of rotor 1 at 95% span (3D-L2F data)

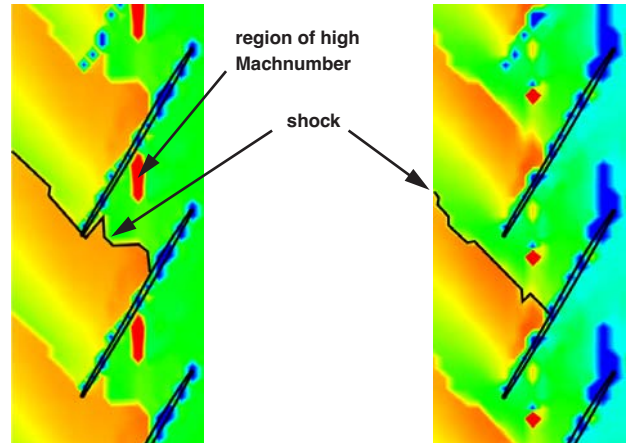


Figure 11 Relative Mach number contour of rotor 3 at 95% span (3D-L2F data)

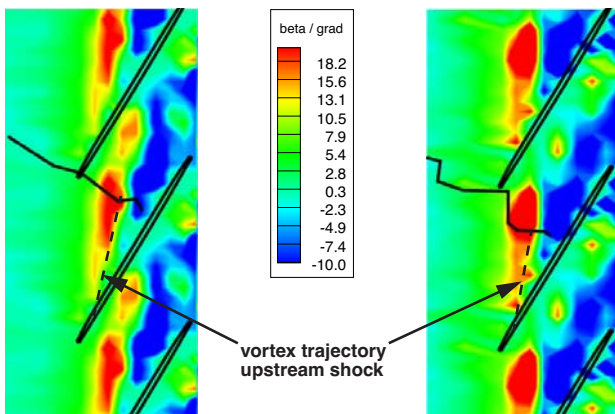


Figure 9 Flow angle beta contour of rotor 1 at 95% span (3D-L2F data)

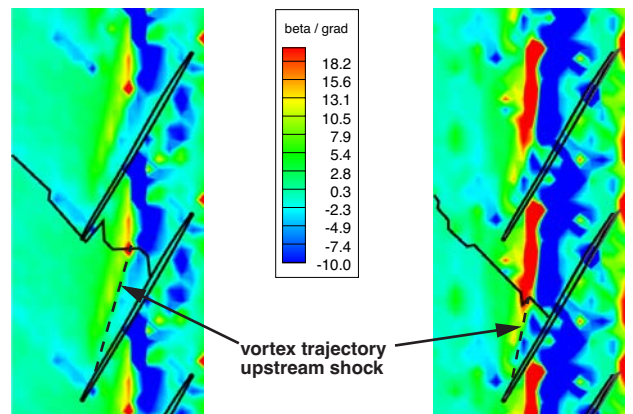


Figure 12 Flow angle beta contour of rotor 3 at 95% span (3D-L2F data)

92.5% span

95% span

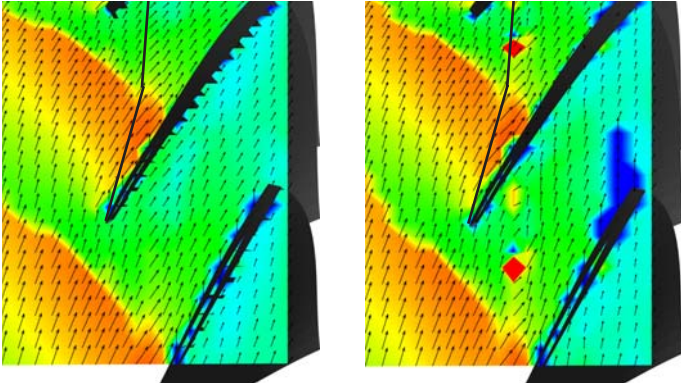


Figure 13 Relative Mach number contours and velocity vectors of rotor 3 at near stall

Trajectory of the tip-leakage vortex

Table 3 lists the length of the tip clearance vortex trajectory upstream of the passage shock non-dimensionalized with blade-spacing and chord. To determine where the vortex emerges from the tip gap and where it intersects the passage shock, all available flow properties like turbulence intensity and flow angles (Fig. 9 and Fig. 11) are taken into consideration.

However, the accuracy of the measured lengths is somewhat lower for rotor 1, because the coarse measurement grid leads to a more uncertain position of the vortex / shock intersection.

The results are in good agreement with the numerical findings shown in [5]. At „peak efficiency“ the forward swept blades of rotor 3, together with the increased chord, lead to a longer distance of the tip clearance vortex until it reaches the passage shock. The analysis of the trajectories of both rotors at „near stall“ conditions, which was not sufficiently possible using the numerical data [5], supports the theory.

At „near stall“ both rotors operate with a shock position that leads to comparable non-dimensional vortex trajectory lengths.

Although both rotors stem from different design philosophies, they also show comparable stall pressure ratios (Fig. 6) and, as shown in [13], both rotors feature spike type stall inception.

Rotor	1		3	
	PE	NS	PE	NS
operat. point	PE	NS	PE	NS
length [mm]	45	41	65	46
length / blade spacing	0,60	0,55	0,76	0,54
length / chord	0,48	0,44	0,59	0,42

Table 3 Length of vortex trajectory from 3D-L2F data

3D Shock structure

It has been of great interest as to how sweep influences the 3D shock structure of an axial transonic compressor rotor. Therefore an attempt was made to visualize the shock from the 3D-L2F data. Usually the shock location is derived from the density gradient. Since the density is not measured by the L2F system and due to the uncertainty caused by calculating a gradient of data on a coarse grid [14], a rather simple approach was chosen.

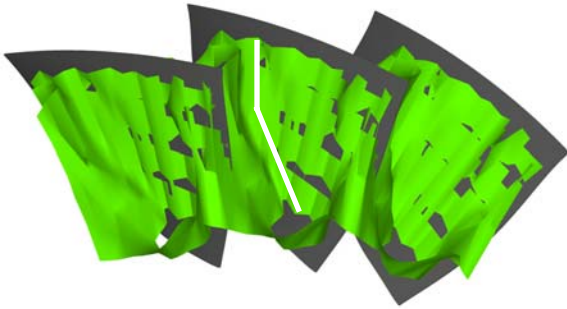
Fig. 14 to Fig. 17 show the 3D iso-surface at which the relative Mach number equals one. Thus the surface is not only limited to the shock, but also covers the suction surface, where the sonic flow field is decelerated in the boundary layer, and the area where the flow gets accelerated above the speed of sound. Each of those figures is accompanied by a view in which the contours of the relative Mach number are drawn on two planes at 50% and 95% span.

Comparing the shock structure of rotor 1 and rotor 3 at „peak efficiency“ (Fig. 14 and Fig. 16, respectively), for rotor 1 the inclination of the shock is more pronounced near the hub. Above mid span the shock has almost no inclination and the shock front appears to be normal to the suction side.

The shock of rotor 3 has only little inclination near the hub. At about 60% span, the shock is abruptly bent downstream into the passage, which could also be seen in the numerical data. Towards the tip the passage shock rights itself and intersects the casing perpendicular, thus forming a concave dent between 60%-95% span in the otherwise almost plane shock front.

At „near stall“ the shocks of both rotors move upstream, the one of rotor 3 even so far that it is detached from the leading edge over the whole span. The dent in the shock front of rotor 3 shrinks and is essentially reduced to a small aft bent at about mid span. Instead, the stronger vortex / shock interaction leads to a hardly noticeable dent.

Iso-surfaces at relative Mach number = 1



Relative Mach number contours

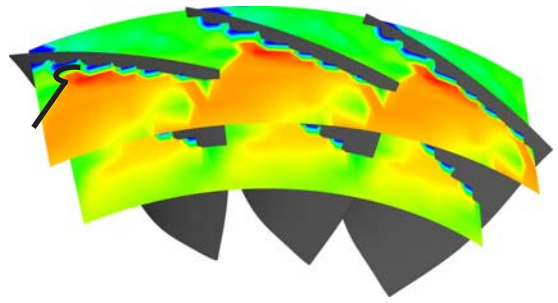


Figure 14 Rotor 1, peak efficiency

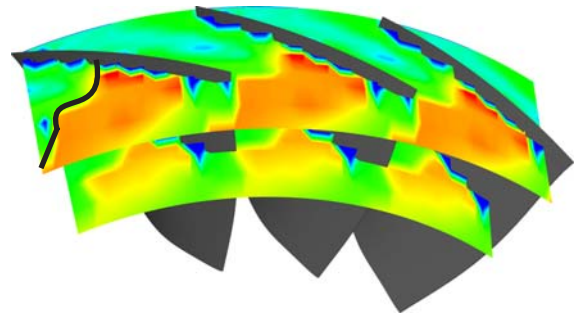
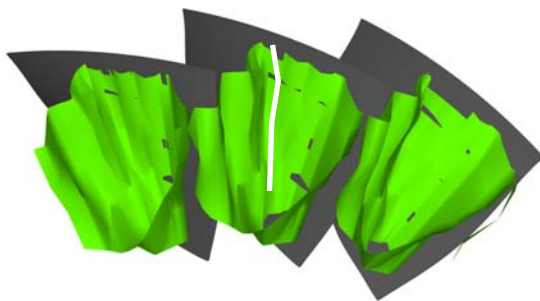


Figure 15 Rotor 1, near stall

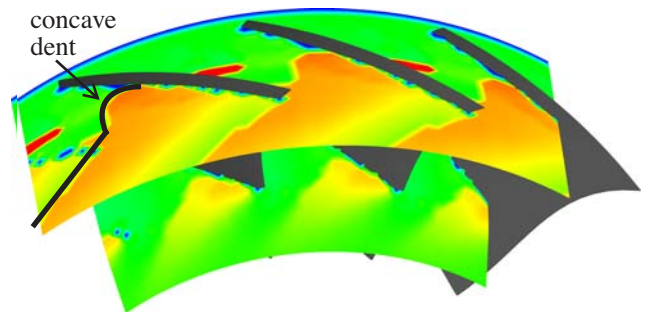
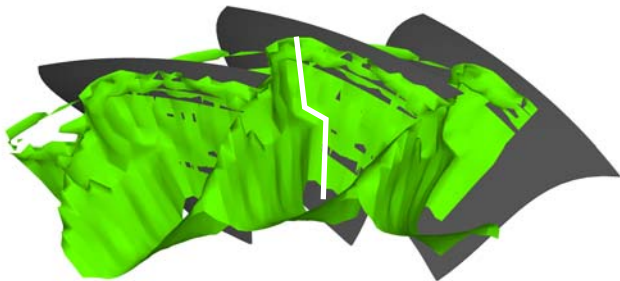


Figure 16 Rotor 3, peak efficiency

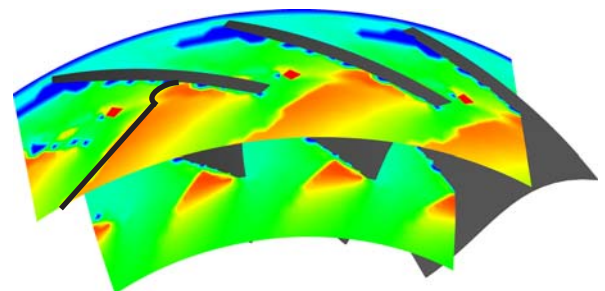
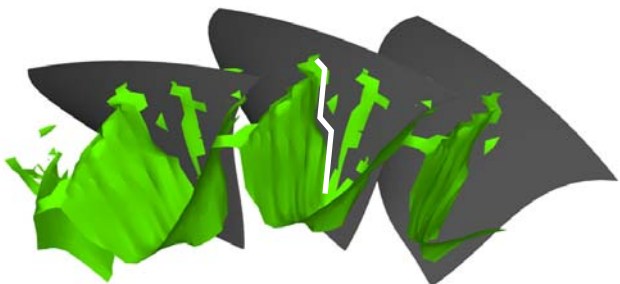


Figure 17 Rotor 3, near stall

Shock / boundary layer interaction

The total-pressure ratio, as determined from total-pressure rakes downstream of the stage, is plotted in Fig. 18 for rotor 3 at „near stall“ in a plane perpendicular to the machine axis. The large area of low total pressure just above mid span led to the question, whether this is caused by flow separation in the stator or in the rotor. In Fig. 19 the radial distribution of the total-pressure ratio at stage exit is plotted for both rotors. Between 40% -70% span, the pressure rise of rotor 3 drops even below that of rotor 1.

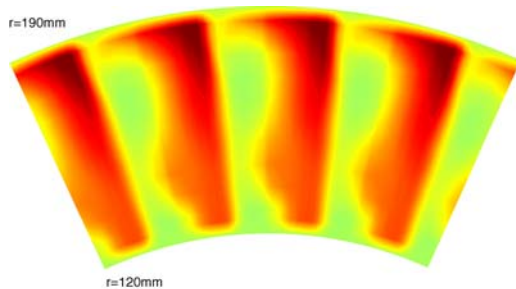


Figure 18 Total-pressure ratio at stage exit near stall (rotor 3)

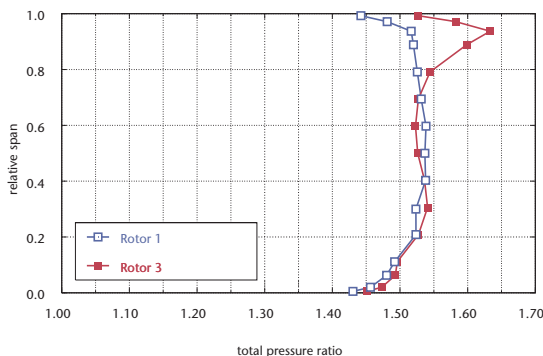


Figure 19 Radial distribution of stage total-pressure ratio at near stall (rotor 1 and rotor 3)

To help assess the situation in the rotor, Fig. 20 shows relative Mach number contours in a plane parallel to the blade tip and located just outside the blade shadow, and in a plane at 60% span, derived from 3D L2F data.

The high pre-shock Mach number between 50% - 80% span indicates a strong, almost normal shock that leads to the forming of a lambda-type shock near the suction surface. This shock / boundary layer interaction is known to thicken up the blade suction surface boundary layer. In our case the region of low Mach number downstream of the shock and its inclination is evidence of boundary layer separation.

Due to the forward sweep and the increased chord of the blade tip, the blade loading is reduced in the tip region, leading to a reduced pre-shock Mach number and thus to a lower blockage of the core flow compared to mid span. Consequently, the rotor performs extremely well above 80% span.

Although it cannot be ruled out that the rotor is the single source of blockage, it is likely that the stator, designed for the expected mass flow range of rotor 1, contributes as well.

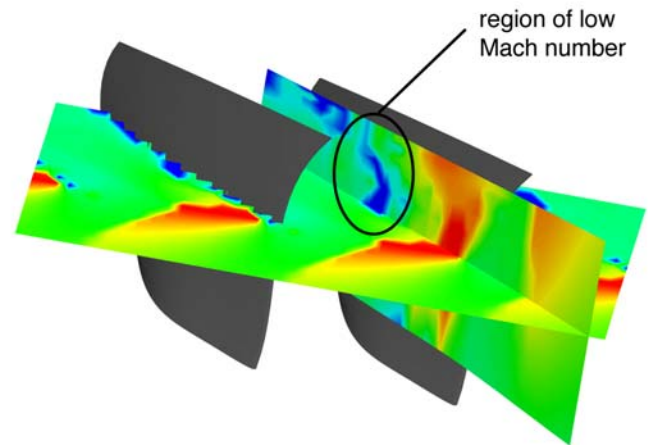


Figure 20 Shock induced boundary-layer separation near stall (3D-L2F data of rotor 3)

CONCLUSIONS

Three-dimensional laser-2-focus measurements are used to investigate the influence of sweep on the flow field of an axial transonic compressor rotor. Comparisons are made with the conventionally-stacked base line rotor.

At „peak efficiency“, the forward swept rotor features a reduced tip clearance vortex, a pronounced shock inclination and an oblique shock front above 50% span. Detailed analyses of the length of the tip clearance vortex upstream of the passage shock underline the role of tip clearance vortex / shock interaction for the onset of stall.

Forward sweep apparently improves the shock structure and together with an increased chord length at blade tip helps to improve the stall margin.

The unloading of the blade tip due to the forward sweep, can lead to high pre-shock Mach numbers at mid span if the compressor is throttled. The resulting separation of the suction side boundary layer might be one reason for the difficulties in obtaining accurate numerical predictions at „near stall“.

ACKNOWLEDGMENTS

This work was funded by the German Ministry of Economics and Labour together with MTU Aero Engines, Munich. The authors are grateful for being able to participate in the project and being able to publish the results.

Special thanks are owed to Martin Müller and Julia Posse for the postprocessing of the 3D-L2F data.

REFERENCES

- [1] Passrucker, H., Engber, M., Kablitz, S., Hennecke, D. K., 2003, „The Effect of Forward Sweep in a Transonic Compressor Rotor“, Proc. 5th European Conference on Turbomachinery (Euroturbo 5), Praha, Czech Republic, 17-22 Mar. 2003.
- [2] Denton, J. D., Xu, L., 1999. „Exploitation of 3D Flow in Turbomachinery“, In: Van den Braembusche, R. A., (Editor), „Turbomachinery Blade Design Systems“, VKI Lecture Series 1999-02, von Karman Institute for Fluid Dynamics.
- [3] Schulze, G., Blaha, C., Hennecke, D. K., Henne, J. M., 1995, „The Performance of a New Axial Single Stage Transonic Compressor“, Proc. 12th Int. Symposium Air Breathing Engines, Melbourne, Australia, Sept. 1995, ISABE 1995-7072.
- [4] Wilke, I., Kau, H.-P., 2002, „A Numerical Investigation of the Influence of Casing Treatments on the Tip Leakage Flow in a HPC Front Stage“, ASME paper GT-2002-30642.
- [5] Kablitz, S., Hennecke, D. K., Passrucker, H., Engber, M., 2003, „Experimental Analysis of the Influence of Sweep on Tip Leakage Vortex Structure of an Axial Transonic Compressor Stage“, Proc. 16th Symposium Air Breathing Engines, Cleveland, OH, USA, 13. Aug. - 5. Sep. 2003, ISABE-2003-1226.
- [6] Kablitz, S., 2003, „Beeinflussung der Spaltströmung von Transsonischen Axialverdichtern durch Forward Sweep“, Dissertation, Fachgebiet Gasturbinen und Flugantriebe, Technische Universität Darmstadt, Darmstadt, Germany.
- [7] Suder, K. L., 1997, „Blockage Development in a Transonic, Axial Compressor Rotor“, ASME paper 97-GT-394.
- [8] Förster, W., 2004, „Das Laser-2-Fokus Velocimeter“, URL: http://www.dlr.de/at/institut/abteilungen/tm_home/messtechniken/l2f_home/l2f_im_detail_ge.html.
- [9] Müller, M., 2003, „3D-Laser-2-Fokus Vermessung des Rotors Nr. 3“, Studienarbeit, Fachgebiet Gasturbinen und Flugantriebe, Technische Universität Darmstadt, Darmstadt, Germany.
- [10] Fritsch, G., Hoeger, M., Blaha, C., Bauer, D., 1997, „Viscous 3D Compressor Simulation on Parallel Architectures“, AIAA paper 97-2876.
- [11] Copenhaver, W. W., Mayhew, E. R., Hah, C., Wadia, A. R., 1994, „The Effect of Tip Clearance on a Swept Transonic Compressor Rotor“, ASME Paper No. 94-GT-363.
- [12] Beheshti, B. H., Teixeira, J. A., Ivey, P. C., Ghorbanian, K., Farhanieh, B., 2004, „Parametric Study of Tip Clearance–Casing Treatment on Performance and Stability of a Transonic Axial Compressor, ASME paper No. 2004-GT-53390.
- [13] Bergner, J., Hennecke, D. K., 2003, „Experimental study of stall-inception of a single-stage transonic compressor“, Proc. 16th Symposium Air Breathing Engines, Cleveland, OH, USA, 13. Aug. - 5. Sep. 2003, ISABE-2003-1081.
- [14] Lovely, D., Haimes, R., 1999, „Shock Detection from Computational Fluid Dynamics Results“, AIAA Paper No. 99-3285.